Research Square

Preprints are preliminary reports that have not undergone peer review.
They should not be considered conclusive, used to inform clinical practice,
or referenced by the media as validated information.

Functional Compensation of Substantia Nigra by Locus Coeruleus in Parkinson's Disease

Qiang Liu
Beijing Institute of Neurosurgery
ZeZhong Zheng
Beijing Institute of Neurosurgery
LuHao Cui
Beijing Institute of Neurosurgery
Pan Wang
Qilu Hospital of Shandong University
Feng Xue
Qilu Hospital of Shandong University
QiChao Cheng
Qilu Hospital of Shandong University
YiLei Xiao
Liaocheng People's Hospital
WenChao Duan
First Affiliated Hospital of Zhengzhou University
Teng Chen
Qilu Hospital of Shandong University
FanGang Meng
fgmeng@ccmu.edu.cn

Beijing Institute of Neurosurgery
RuiHua Hou
University of Southampton

Research Article

Keywords: Neuromelanin, Locus Coeruleus, Parkinson's Disease, Substantia nigra, Network-level analysis, Hidden Markov model

Posted Date: July 2nd, 2026

DOI: https://doi.org/10.21203/rs.3.rs-9983548/v1

License: This work is licensed under a Creative Commons Attribution 4.0 International License.
Read Full License

Additional Declarations: No competing interests reported.

Abstract

Neuromelanin is abundant in locus coeruleus (LC), yet its loss occurs across multiple neurodegenerative diseases. However, the role of LC in Parkinson's disease (PD) remains controversial. In this study, we recruited 37 patients with PD, 18 patients with mild cognitive impairment (MCI), and 27 healthy controls (HC). All participants underwent clinical assessments and multimodal MRI acquisition. Neuromelanin-sensitive MRI (NM-MRI) was used to quantify neuromelanin loss in substantia nigra pars compacta (SNpc) and LC, while 3D T1-weighted imaging and BOLD-fMRI were employed to assess structural and functional brain networks, respectively. Voxel-based and surface-based morphometry revealed PD was primarily associated with impairments in visual, control, and somatomotor network, whereas MCI predominantly involved dysfunction of default mode network. The contrast-to-noise ratio in both SNpc and LC was significantly reduced in PD. In contrast, MCI patients showed no apparent SNpc alterations but exhibited significant neuromelanin loss in LC. Graph theory analysis demonstrated pathological hyper-efficiency in the functional connectivity network of PD, with compensatory or maladaptive nodal changes varying across disease-related networks. Network-level analysis indicated that the effects of SNpc pathology on cortical morphological similarity and functional connectivity were complementary during PD progression. Moreover, LC exerted a functional compensatory influence on SNpc in PD, while SNpc showed particularly strong coupling with cortical morphological similarity in visual network. Hidden Markov model analysis further revealed PD was characterized by a reduced number of dynamic brain network states and a decreased state-switching rate, which was more strongly modulated by LC pathology. Collectively, these findings suggest that LC plays a substantial functional compensatory role for substantia nigra in PD.

Introduction

Current understanding of Parkinson's disease (PD) pathology is no longer limited to damage of dopaminergic neurons in the substantia nigra pars compacta (SNpc). Increasing evidence demonstrates that noradrenergic neurons in the locus coeruleus (LC) of the pons also undergo apoptosis, often preceding SNpc damage[1, 2]. Anatomically, LC is a nucleus located adjacent to the fourth ventricle in the rhomboid fossa of the brainstem, with axonal projections extending throughout almost the entire brain[3]. It participates in regulating diverse brain functions, including wakefulness, pain modulation, and metabolic processes, and plays a crucial role in cognitive-emotional regulation and learning and memory[4]. Due to its anatomical proximity to cerebrospinal fluid, LC axons are particularly susceptible to toxins and inflammatory factors, making LC dysfunction widespread in neurodegenerative diseases. Research indicates that LC damage closely correlates with apathy and cognitive impairment in PD patients. Clinical trials utilizing atomoxetine, as a selective noradrenaline reuptake inhibitor, have shown that it can partially compensate for impaired LC function, improving conflict-control abilities in PD patients[5]. Additionally, LC dysfunction significantly contributes to the pathogenesis of rapid eye movement sleep behavior disorder (RBD) in PD, particularly through sub-coeruleus regions involved in sleep regulation[6]. Furthermore, the loss of LC's noradrenergic neurons disrupts cortical-striatal-thalamic circuit activity, leading to sensory abnormalities and impaired pain localization[7]. Concurrently,

LC-mediated descending inhibitory control on spinal pain pathways becomes dysfunctional, causing increased pain sensitivity[8, 9]. Collectively, these findings underscore the importance of LC pathology in the manifestation of non-motor symptoms in PD.

Cognitive impairment is common in PD, with considerable heterogeneity in severity, and its prevalence increases with the duration of motor symptoms[10]. Studies focusing on newly diagnosed PD patients have reported that the prevalence of mild cognitive impairment (MCI) is approximately 10%~35%[11, 12]. Moreover, severe dementia often surpasses motor symptoms as the primary cause of disability and mortality in PD. At present, neither pharmacological nor surgical treatments offer effective relief for PD-related cognitive impairment, and there are also notable limitations in the clinical diagnosis and differential diagnosis of PD dementia. Previous studies[13] have shown that in PD-MCI, dopaminergic depletion is largely confined to the basal ganglia, while the limbic system and neocortical regions are relatively spared. Only with progression from MCI to dementia does dopaminergic loss gradually extend throughout the brain. In contrast, noradrenergic deficits in LC are already widespread across the brain even in cognitively normal PD patients, with severity increasing as MCI progresses. Earlier basic research has further demonstrated a protective role of LC on dopaminergic neurons. Firstly, LC exerts direct protective effects. In the early stages of PD, norepinephrine (NE), as a neurotransmitter, can partially compensate for dopamine (DA) deficiency[14]. NE release facilitates the clearance of extracellular superoxide, thereby reducing its neurotoxic effects. Axons of LC neurons can also uptake MPP^+, the toxic metabolite of MPTP, buffering its toxicity to dopaminergic neurons[15]. In addition, non-noradrenergic neurons within LC secrete neuroprotective substances, such as growth hormone–releasing peptides and brain-derived neurotrophic factor (BDNF)[16]. Second, LC modulates neurons in the substantia nigra through NE signaling. Studies have shown that dopaminergic and glutamatergic neurons express adrenergic receptors, among which α2 receptors play a key role in mediating interactions between NE and dopaminergic neurons[17]. Activation of α2 receptors by NE can enhance DA synthesis and storage and accelerate DA metabolism[14]. Third, LC exerts protective effects on dopaminergic neurons via glial cells. Otto et al. found that NE increases the synthesis of epidermal growth factor (EGF) in glial cells, which has a pronounced protective effect on dopaminergic neurons[18]. Numerous studies have also suggested that NE can upregulate the expression of nerve growth factor (NGF). Furthermore, NE itself has anti-inflammatory properties. Collectively, these findings suggest that in PD, LC may play a compensatory role for the substantia nigra within large-scale brain functional networks.

Neuromelanin is formed through the oxidation of cytosolic dopamine, norepinephrine, or other catecholamines by tyrosinase, is stored in lysosomes, and forms chelates with metal ions such as iron, copper, and zinc, as well as with lipids[19]. This endows neuromelanin with paramagnetic properties in a magnetic field, leading to T1 relaxation shortening and hyperintense signals on T1-weighted images. Because dopaminergic neurons in the SNpc and noradrenergic neurons in the LC are rich in neuromelanin, magnetic resonance imaging (MRI) enables visualization of these structures using neuromelanin-sensitive MRI sequences[20, 21]. In recent years, resting-state functional MRI based on blood oxygen level–dependent (BOLD) signals has provided a noninvasive means to detect differences in neural activity between patients with central neurodegenerative diseases and healthy individuals,

thereby facilitating the investigation of relationships between specific symptoms and alterations in functional networks[22, 23]. In addition, owing to its high spatial resolution, isotropic voxels, and excellent tissue contrast, 3D T1-weighted imaging has become an important tool for detecting subtle structural changes in the PD brain[24, 25]. In particular, structural covariance network analysis based on cortical morphology can characterize intrinsic properties of brain development and aging, as well as the extrinsic effects of environmental factors and chronic diseases on brain structure, offering a novel perspective for brain network analysis. However, structural covariance networks rely on a single metric to describe group-level changes and cannot capture multi-metric, individual-level relationships in cortical morphology[26]. To address this limitation, a novel approach, morphological similarity network (MSN), has been proposed.

How do impairments in the dopaminergic system of SNpc and the noradrenergic system of LC influence brain networks? The present study integrates multimodal MRI data, including neuromelanin-sensitive MRI, 3D T1-weighted imaging, and BOLD-fMRI, to comprehensively investigate changes in SNpc and LC among PD and MCI patients. From both structural and functional perspectives, we examine the characteristics of brain networks in PD and MCI, with a particular focus on elucidating how pathological alterations in SNpc and LC affect morphological similarity networks and functional connectivity networks, and on identifying potential pathological circuits. Through this approach, we aim to explore the important role of neuromelanin-sensitive MRI in the prediction and evaluation of PD, cognitive impairment, and other neurodegenerative diseases.

Methods

Subjects and Assessments

This study was conducted in accordance with the Declaration of Helsinki. The study protocol was reviewed and approved by the Ethics Committee of Qilu Hospital. Informed consent was obtained from all participants involved in various assessments. From September 2023 to December 2024, a total of 37 patients with primary Parkinson’s disease (PD), 18 patients with mild cognitive impairment (MCI), and 27 healthy controls (HC) participated in this study. All subjects were recruited from outpatient and inpatient units of the Departments of Neurology and Neurosurgery. Clinical scale assessments for all patient groups were conducted 12 hours after medication withdrawal and were completed in one session wherever possible. All subjects underwent evaluations using the Montreal Cognitive Assessment (MoCA)[43], Hamilton Depression Scale (HAMD)[44], and Hamilton Anxiety Scale (HAMA)[45]. Both PD and MCI patients were further assessed using the Clinical Dementia Rating (CDR)[46], Neuropsychiatric Inventory (NPI)[47], Alzheimer's Disease Assessment Scale-Cognitive Subscale (ADAS-cog)[48], and Activities of Daily Living (ADL)[49]. PD patients were additionally evaluated with the Unified Parkinson’s Disease Rating Scale Part III (UPDRS-III)[50] and Non-Motor Symptoms Scale (NMSS)[51]. All scale assessments were independently completed and recorded by two physicians. (Table 1)

Table 1

Group Information and Clinical Characteristics. #: chi-square test; PD: Parkinson's disease. MCI: Mild cognitive impairment. P_1: PD versus Healthy Subjects; P_2: MCI versus Healthy Subjects. All data were reported as mean ± SD.

Age (years)	**Healthy Subjects(n = 27)**	**PD(n = 37)**	**MCI(n = 18)**	***P* value**
	55.41 ± 14.18	**59.43 ± 10.74**	**70.78 ± 7.94**	***P*$_1$=0.19 *P*$_2$ < 0.05**
Gender (male/female)	10/17	13/24	4/14	$P^{\#}$=0.54
Duration of disease (years)	-	7.51 ± 3.88	3.28 ± 2.93	-
MoCA	27.42 ± 1.26	23.54 ± 4.76	12.00 ± 5.44	P_1<0.05 P_2 < 0.05
HAMD	4.91 ± 2.72	12.54 ± 6.04	10.39 ± 6.42	P_1<0.05 P_2 < 0.05
HAMA	5.14 ± 3.51	12.46 ± 4.27	19.06 ± 9.32	P_1<0.05 P_2 < 0.05
ADL(Barthel)	-	71.23 ± 14.38	61.72 ± 11.3	P_2<0.05
Hoehn-Yahr stage	-	2.86 ± 0.89	-	-
UPDRS Part	-	45.41 ± 22.35	-	-
NMSS	-	48.32 ± 22.74	-	-
CDR	-	0.45 ± 0.48	0.88 ± 0.63	P_2<0.05
NPI	-	25.52 ± 10.08	30.39 ± 17.11	P_2<0.05
ADAS-cog	-	10.25 ± 9.86	26.33 ± 10.52	P_2<0.05

Table 1
Group Information and Clinical Characteristics

Age (years)	**Healthy Subjects(n = 27)**	**PD(n = 37)**	**MCI(n = 18)**	***P* value**
	55.41 ± 14.18	**59.43 ± 10.74**	**70.78 ± 7.94**	**P_1=0.19 P_2 < 0.05**
Gender (male/female)	10/17	13/24	4/14	$P^{\#}$=0.54
Duration of disease (years)	-	7.51 ± 3.88	3.28 ± 2.93	-
MMSE	28.60 ± 1.13	24.48 ± 4.31	13.00 ± 5.43	P_1<0.05 P_2 < 0.05
MoCA	27.42 ± 1.26	23.54 ± 4.76	12.00 ± 5.44	P_1<0.05 P_2 < 0.05
HAMD	4.91 ± 2.72	12.54 ± 6.04	10.39 ± 6.42	P_1<0.05 P_2 < 0.05
HAMA	5.14 ± 3.51	12.46 ± 4.27	19.06 ± 9.32	P_1<0.05 P_2 < 0.05
ADL(Barthel)	-	71.23 ± 14.38	61.72 ± 11.3	-
Hoehn-Yahr stage	-	2.86 ± 0.89	-	-
UPDRS Part Ⅲ	-	45.41 ± 22.35	-	-
NMSS	-	48.32 ± 22.74	-	-
CDR	-	-	0.88 ± 0.63	-
NPI	-	-	30.39 ± 17.11	-
ADAS-cog	-	-	26.33 ± 10.52	-

#: chi-square test; PD: Parkinson's disease. MCI: Mild cognitive impairment. P_1: PD versus Healthy Subjects; P_2: MCI versus Healthy Subjects. All data were reported as mean ± SD.

MRI Scanning

All MRI scans were performed using a 3.0 Tesla GE SIGNA Architect scanner. All subjects underwent scanning with standardized protocols including 3D-T1 imaging, NM-MR, and BOLD-fMRI. The NM-MRI localization box was positioned on T1-weighted sagittal images, extending from the splenium of the

corpus callosum to the lower edge of the pons, perpendicular to the base of the fourth ventricle, fully covering midbrain and pontine structures. Routine T2-weighted, FLAIR, and diffusion-weighted imaging (DWI) sequences were also performed to exclude central nervous system disorders such as ischemic lesions, vascular malformations, or tumors. Detailed sequence parameters were as follows:

3D-T1: repetition time (TR) = 7.5 ms, echo time (TE) = 2.9 ms, slice thickness = 1 mm, flip angle = 12°, number of slices = 160, field of view (FOV) = 25.6 cm × 25.6 cm, matrix size = 256 × 256, acquisition time = 2 min 35 s.

NM-MRI: fast spin echo (FSE), echo train length = 2, TR/TE = 600/14 ms, slice thickness = 3.0 mm without gap, number of slices = 12, FOV = 24.0 × 24.0 cm, matrix size = 512 × 320, number of excitations (NEX) = 5, acquisition time = 9 min 44 s.

BOLD-fMRI: TR = 2000 ms, TE = 35 ms, slice thickness = 4 mm, flip angle = 90°, FOV = 24.0 cm × 24.0 cm, matrix size = 64 × 64, 240 time points, 36 axial slices per time point, acquisition time = 8 min.

MRI Data Processing

For NM-MRI, ITK-SNAP software (https://www.itksnap.org) was used to measure signal intensity (SI) from three consecutive slices of SNpc and two consecutive slices of LC. The superior cerebellar peduncle was used as a reference for SNpc's measurement, while the pontine tegmentum served as the reference for LC. Each region's signal intensity was manually segmented three times, with the mean value calculated. The contrast-to-noise ratio (CNR) of each nucleus was calculated as $(SI_{target} - SI_{reference}) / (SI_{reference})$, resulting in CNR of SNpc (SNpc_CNR) and CNR of LC (LC_CNR). Three physicians blinded to participant information conducted these measurements independently, with two performing initial segmentation and the third physician verifying and averaging results.

3D T1-weighted images were preprocessed using CAT12 software after origin correction, (https://neuro-jena.github.io/cat), including tissue segmentation, spatial normalization, surface reconstruction, and resampling. This pipeline yielded multiple morphometric measures, such as gray matter volume, cortical thickness, sulcal depth, fractal dimension, gyrification index, and Toro's gyral complexity (ToroGI20 mm). Both voxel-based morphometry (VBM) and surface-based morphometry (SBM) analyses were subsequently performed. In addition, these metrics were extracted using the Schaefer cortical atlas (400 ROIs)[27] to enable subject-level construction of morphological similarity networks.

For BOLD fMRI data, preprocessing was first conducted using the DPARSFA toolbox (https://rfmri.org/DPARSF), including removal of the first five time points, slice timing correction, head motion correction, and origin correction. Subjects with head motion exceeding 2 mm in translation or 2° in rotation were excluded. The EPI images were then spatially normalized using the DARTEL approach. Subsequently, the normalized data underwent linear trend removal, nuisance covariate regression, and temporal filtering. Time series were extracted from the preprocessed 4D data using the same Schaefer

template, and individual static functional connectivity (FC) matrices were constructed. Graph measurements of the resting-state FC networks were computed using the Brain Connectivity Toolbox (BCT)[28]. Furthermore, the HMM-MAR toolbox (https://github.com/OHBA-analysis/HMM-MAR) was applied to construct hidden Markov models (HMM) for three groups of participants[29]. The optimal number of network states was determined, and summary statistics, like state switching rate, state transition probability, and mean state activation, were calculated. (Fig. 1.)

Statistical Analysis

Differences in age and neuropsychological scale scores among PD, MCI, and healthy control (HC) were assessed using Mann–Whitney U test, while sex distribution across three groups was compared using chi-square test. Smoothed gray matter volume maps were used to perform two-sample t-tests between PD, MCI and HC, and brain regions showing significant differences were identified after correction for multiple comparisons. Similarly, resampled cortical thickness data were subjected to two-sample t-tests between groups, with multiple-comparison correction applied to determine cortical regions with significant group differences. Graph measure calculation derived for all groups, including global metrics such as small-world property, clustering coefficient, and global efficiency, as well as nodal metrics such as nodal degree and nodal efficiency, were compared using t-tests, with false discovery rate (FDR) correction. In addition, the Network-Level Analysis (NLA) toolbox was employed to conduct edge-wise Pearson correlation analyses between SNpc_CNR/LC_CNR and MSN matrices (after Fisher r-to-z transformation) for each group[30]. (Fig. 1.) Correlation matrices were binarized based on statistical significance, and network-level enrichment of significant correlations within the Yeo 17-network parcellation was evaluated using the hypergeometric test and permutation testing (10,000 iterations) under full-connectome level. Westfall-Young ranking correction and FDR correction were applied to control for multiple-comparison errors. The same analytical framework was applied to FC network analysis. For the HMM results, group differences in state switching rates were assessed using t-tests. Furthermore, regression models were constructed to examine the associations between SNpc_CNR/LC_CNR and state switching rates. All of the above statistical analyses were performed based on MATLAB R2023b and SPM12 software package.

Results

VBM and SBM Analyses

Voxel-based morphometry (VBM) revealed that, compared with controls, PD patients exhibited gray matter volume reductions mainly in the midbrain and thalamus, whereas MCI patients showed predominant gray matter loss in the middle frontal gyrus and hippocampus. All VBM results survived FWE cluster-level correction ($P < 0.001$). Surface-based morphometry (SBM) demonstrated that PD patients had significantly reduced cortical thickness in the occipital lobe, central regions, and superior frontal gyrus (FWE voxel-level correction, $P < 0.05$). In contrast, MCI patients showed cortical thinning primarily in the precuneus, middle temporal gyrus, and inferior temporal gyrus (FWE cluster-level

correction, $P < 0.001$). These results suggest that PD is mainly associated with impairments in visual, control, and somatomotor networks, whereas MCI predominantly involves dysfunction of default mode network. (Fig. 2.)

Changes in SNpc and LC on NM-MRI

Compared with healthy controls (HC), neuromelanin content in both substantia nigra pars compacta (SNpc) and locus coeruleus (LC) was significantly reduced in patients with Parkinson's disease (PD)[21]. In contrast, within MCI group, no obvious change was observed in SNpc, whereas neuromelanin is significantly reduced in LC. These findings indicated that LC pathology is already present in both PD and MCI, whereas SNpc damage is evident in PD but not in MCI. (Fig. 3.)

Graph Theory Analysis

Global network metrics showed no significant differences between MCI and HC. In contrast, PD patients exhibited a significant reduction in the global clustering coefficient compared with HC ($P < 0.05$), whereas the normalized clustering coefficient was increased. In addition, global efficiency and small-worldness were also elevated in PD relative to controls, indicating a pathological hyper-efficiency of the functional connectivity network in PD. At the nodal level, compared with HC, the number of regions showing altered nodal degree and nodal efficiency was markedly less in MCI than in PD. Moreover, in both MCI and PD, regions exhibiting differences in nodal degree and nodal efficiency showed a high degree of spatial overlap, suggesting strong interdependence between the two nodal measures. Specifically, in MCI, nodal degree and nodal efficiency were mainly increased within CN and DMN. In PD, these increases were also widespread in CN and DMN, but significant reductions were observed in Vis, SMN and DAN. These findings indicate that compensatory or maladaptive changes in network nodes are not uniform across disease-related networks. (Fig. 3.)

Network-Level Analysis

At the whole-brain connectivity level, after applying Westfall-Young ranking correction and FDR correction, we found that in HC, SNpc was mainly associated with cortical morphological similarity between SMN and Vis or VAN. In PD, SNpc-related effects shifted to morphological similarity between DAN and Vis, as well as within DMN. In MCI, SNpc primarily influenced morphological similarity between VAN and Vis or LIM. Regarding LC, it mainly affected morphological similarity between DAN and Vis or VAN in HC. In PD, LC predominantly influenced morphological similarity within DAN and between DAN and VAN. In contrast, in MCI, LC showed no significant effects on morphological similarity across networks.

The same analytical framework was applied to FC networks. In HC, SNpc mainly influenced FC between DAN and Vis or DMN. In PD, SNpc predominantly affected FC within SMN. In MCI, SNpc mainly

modulated functional interactions between DMN and SMN or CN. Conversely, in HC, LC primarily influenced FC between DMN and LIM or temporoparietal network (TPN). In PD, LC mainly affected functional interactions between DMN and SMN or TPN. In MCI, LC predominantly influenced FC between DMN and LIM or CN, as well as between TPN and LIM.

Taken together, the effects of SNpc and LC on cortical morphological similarity and functional connectivity are not fully synchronized. In healthy individuals, SNpc mainly influences SMN in terms of morphological similarity, whereas its functional effects are primarily related to DAN. This pattern is reversed in PD, and SNpc is mainly associated with DAN and DMN in morphological similarity, but is functionally closely linked to SMN. Meanwhile, LC maintains close associations with both attention networks in morphological similarity in HC and PD, and also preserves its influence on functional interactions between DMN and TPN. In PD, LC additionally affects interactions between DMN and SMN, suggesting a potential compensatory role of LC for SNpc's dysfunction. In contrast, in MCI patients, SNpc preferentially involves VAN in structural similarity and DMN in functional connectivity, whereas LC shows no significant association with cortical morphological similarity, suggesting that cortical structural alterations in primary cognitive impairment may be independent of LC pathology. (Fig. 4.)

Hidden Markov Model Analysis

Using the HMM-MAR toolbox, variational Bayesian inversion of hidden Markov models (HMM) was performed on time series from all 400 parcels for each group. State parameters were optimized across 50 repeated cycles, and mean variational free energy and mean fractional occupancy were calculated for each state. In HC and MCI, the models showed clear convergence, with mean variational free energy exhibiting a minimum as a function of state number, corresponding to K = 10 and K = 8, respectively. In contrast, in PD patients, mean variational free energy increased monotonically with increasing K. Therefore, we further computed the relative free energy gain between adjacent state numbers (ΔFE/FE) to evaluate marginal benefits[29]. As K increased, marginal gains rapidly plateaued beyond K = 6 ~ 8, indicating that adding more states yielded minimal improvement in model fit. Examination of mean fractional occupancy revealed that when K exceeded this range, the model began to generate rare states with extremely low occupancy, suggesting over-fragmentation of existing states rather than the emergence of new stable brain dynamic patterns. Considering marginal fit improvement, state occupancy stability, and interpretability, the optimal number of states for the PD model was set to K = 8 rather than simply selecting the maximum K with the lowest free energy.

These findings further indicate that, compared with HC, both MCI and PD patients exhibit a reduced number of resting-state network states and significantly decreased state switching rates. Regression analyses revealed a significant positive association between SNpc_CNR and state switching rate in healthy controls ($R^2 = 0.15$, $P = 0.048$). In PD group, however, a significant positive association was observed between LC_CNR and state switching rate ($R^2 = 0.11$, $P = 0.045$). No significant associations were found between SNpc_CNR or LC_CNR and state switching rate in MCI patients. In addition, although transitions between different states were possible in all three groups, transition probabilities

were asymmetric. Most states were characterized by mixed patterns of network activation and deactivation, with only a small number of states in HC and MCI showing global activation across networks. (Fig. 5.)

Discussion

The clinical manifestations of Parkinson's disease (PD) are mediated by the combined damage to dopaminergic neurons in the substantia nigra pars compacta (SNpc) and noradrenergic neurons in the locus coeruleus (LC). However, LC degeneration is not specific to PD; varying degrees of LC pathology have also been reported in several cognitive disorders, such as dementia with Lewy bodies and Alzheimer's disease[31, 32]. In the present study, we likewise identified LC impairment in a subset of patients with mild cognitive impairment (MCI). Naturally, pathological changes in brainstem nuclei are expected to be accompanied by alterations in cerebral morphology. On the one hand, we observed significant volume reductions in the midbrain and thalamus in PD compared with healthy controls, which is consistent with previous reports[33]. In contrast, the MCI's model revealed bilateral hippocampal atrophy and focal volume loss in frontal regions[33]. On the other hand, although the cerebral cortex, the highest-level central nervous system responsible for regulating and controlling bodily functions, is closely related to development and aging, it undergoes further degeneration in neurodegenerative diseases. We found marked cortical atrophy in the frontoparietal central regions and occipital cortex in PD patients, which corroborates the characteristic motor and visuospatial impairments in PD[34, 35]. In MCI patients, cortical thinning was mainly observed in the precuneus and focal temporal regions, areas that are critically involved in cognitive information processing[36]. Accordingly, we propose that bilateral hippocampal volume and precuneus cortical thickness may serve as imaging markers for identifying PD patients with comorbid MCI.

In the resting state, the human brain can be organized into several functional networks, including the visual network (Vis), somatomotor network (SMN), dorsal attention network (DAN), Ventral attention network (VAN), limbic network (LIM), control network (CN), default mode network (DMN), and temporoparietal network (TPN)[27, 37]. These subnetworks play fundamental roles in neurodegenerative diseases[38] and interact with one another to confer small-world properties, topological stability, and high efficiency to brain information processing. We found that global network metrics in MCI were largely comparable to those in healthy controls, whereas PD patients exhibited a significant reduction in the global clustering coefficient. Paradoxically, normalized clustering coefficient, global efficiency, and small-worldness were increased in PD, suggesting a state of pathological hyper-efficiency in the functional brain network[39]. Two potential explanations may account for this phenomenon. First, brain network communication efficiency may exhibit adaptive or elastic regulation; as the disease progresses, loss of compensation or excessive compensation may manifest as pathological hyper-efficiency. Second, long-term use of medications such as levodopa and dopamine receptor agonists may drive PD brain networks toward a persistently high-efficiency state[39]. At the nodal level, PD showed more extensive abnormalities than MCI. In both PD and MCI, nodal degree and nodal efficiency were significantly increased in CN and DMN, but markedly reduced in Vis, SMN and DAN. This pattern may indicate that

non-motor symptoms emerge earlier and more mildly, whereas motor symptoms appear later and more severely in PD, highlighting that network efficiency compensation during disease progression is neither balanced nor uniform in direction.

Structural covariance network (SCN) characterizes coordinated patterns of brain structural variation at the group level and are commonly used to assess the synchrony of developmental, aging, or pathological changes across regions based on measures such as cortical thickness and gray matter volume. A core assumption of SCN is that functionally or developmentally related brain regions exhibit coordinated structural changes, allowing SCN to partially recapitulate functional connectivity patterns[40]. However, traditional SCN is constructed at the group level using a single metric and thus cannot comprehensively capture individual-level network organization. To address this limitation, morphological similarity network (MSN) has been proposed. MSN is based on two key assumptions: first, that macroscopic structural MRI similarity reflects microscopic similarities in cellular and/or myelin architecture; and second, that anatomically similar regions are more likely to be interconnected via axonal pathways, making MSN a surrogate marker of connectivity[26]. In the present study, using network-level analyses, we compared the associations between SNpc and LC contrast-to-noise ratios (CNRs) and both MSN and functional connectivity network (FCN), identifying network nodes with significant associations. We found that the networks influenced by SNpc in PD and healthy controls were essentially opposite. Specifically, in healthy controls, SNpc primarily modulated structural similarity between SMN and other networks, as well as functional connectivity between DAN and other networks. In PD, however, SNpc was more strongly associated with SMN at the functional connectivity level, while exerting greater influence on DAN and other networks at the morphological similarity level. This pattern suggests a complementary shift between cortical structure and function associated with SNpc during PD progression. In contrast, LC showed consistent effects on MSN across both groups, but its influence on FCN in PD shifted from DMN-LIM to DMN-SMN coupling, implying a compensatory functional role of LC for SNpc dysfunction. Conversely, in MCI, LC showed no significant association with MSN, indicating that cortical structural alterations in cognitive impairment may not be directly related to LC pathology. Instead, SNpc effects on MSN shifted toward coupling between VAN and LIM, while both SNpc and LC predominantly influenced FCN through coupling between DMN and CN or other networks. This suggests that DMN dysfunction may represent a key substrate of cognitive impairment. Notably, across all three groups, the structural similarity coupling between Vis and other networks was closely associated with SNpc, suggesting a particularly strong linkage between SNpc and visual network cortical morphology.

Hidden Markov model (HMM) represents a promising approach for characterizing the dynamic properties of spatial brain states[41]. Unlike traditional sliding-window approaches to dynamic connectivity, HMMs preserve the full temporal resolution of time series and reduce insensitivity to transient changes[42]. HMMs assume that observed time series arise from discrete latent spatial states that can recur at any time point and can be inferred from the probability distributions of observations. Previous HMM studies in healthy populations have shown that spatiotemporal brain activity patterns are related to behavioral traits and emotion elicited during movie viewing, and alterations in HMM-derived brain dynamics have been reported in post-traumatic stress disorder, schizophrenia, and Alzheimer’s

disease[42]. In this study, we used metrics such as free energy (FE) and fractional occupancy (FO) to determine the optimal number of states (K) for HMM construction in the three groups. We observed clear FE minima only in the HC and MCI groups, corresponding to K = 10 and K = 8, respectively. In contrast, FE failed to converge in PD, indicating a disruption of latent functional states within the PD brain network. To address this, we proposed a marginal free-energy gain approach to select an interpretable optimal K = 8 for PD, recognizing that excessive state numbers would undermine the goal of obtaining a low-dimensional and interpretable representation. We found that states could transition between one another in all three groups, with asymmetric transition probabilities. Moreover, most states exhibited mixed patterns of network activation and deactivation rather than uniform activation. Focusing on state switching rate, defined as the average number of state activations per unit time, we observed a reduction in PD, whereas MCI showed little change. Regression analyses relating CNR to switching rate revealed that SNpc played a dominant role in healthy controls, LC exerted the primary influence in PD, and neither was significantly associated in MCI. These findings further support the notion that LC may functionally compensate for SNpc damage during PD progression and suggest that LC pathology may be more severe than SNpc degeneration in PD.

Taken together, this study has several notable limitations. Firstly, it is a small-sample, single-center, cross-sectional study, and most analyses are driven by imaging data and statistical modeling without direct clinicopathological validation, limiting the interpretability of clinical applicability. Second, due to the relatively long scanning protocol, diffusion tensor imaging data were not acquired. In addition, subtle head motion and anxiety-related factors in some patients may have introduced noise into the images, potentially affecting the reliability of the results. Future multicenter studies with larger sample sizes and longitudinal designs are required to further validate and extend these findings.

Conclusion

Neuromelanin loss in the substantia nigra pars compacta (SNpc) represents a relatively specific pathological hallmark of Parkinson’s disease (PD), whereas degeneration of the locus coeruleus (LC) is not unique to PD and is also observed in other neurodegenerative disorders, including those associated with cognitive impairment. The functional brain network in PD exhibits pathological hyper-efficiency, which may arise from excessive compensatory adaptation of network regulation as well as the long-term use of dopaminergic medications. Importantly, compensatory changes in network efficiency are often imbalanced and non-uniform in direction. During PD progression, the effects of SNpc pathology on cortical morphological similarity and functional connectivity appear to be complementary. Moreover, LC exerts a compensatory functional influence on SNpc in PD, and SNpc shows particularly strong coupling with the cortical morphological similarity of visual network. Compared with healthy individuals, neurodegenerative diseases such as PD are characterized by a reduced number of dynamic brain network states; in addition, PD is associated with a decreased state switching rate, which is more strongly modulated by LC pathology. These findings suggest that pathological alterations of the locus coeruleus may represent an important biomarker for the onset and progression of Parkinson’s disease.

Abbreviations

ADAS-cog
Alzheimer’s Disease Assessment Scale-Cognitive Subscale
ADL
Activities of Daily Living
BDNF
Brain-derived neurotrophic factor
BOLD
Blood oxygen level-dependent
BOLD-fMRI
Blood oxygen level-dependent functional magnetic resonance imaging
CAT12
Computational Anatomy Toolbox 12
CDR
Clinical Dementia Rating
CN
Control network
CNR
Contrast-to-noise ratio
DA
Dopamine
DAN
Dorsal attention network
DARTEL
Diffeomorphic Anatomical Registration Through Exponentiated Lie Algebra
DMN
Default mode network
DWI
Diffusion-weighted imaging
EGF
Epidermal growth factor
EPI
Echo-planar imaging
FC
Functional connectivity
FCN
Functional connectivity network
FDR
False discovery rate

FE
Free energy
FLAIR
Fluid-attenuated inversion recovery
FO
Fractional occupancy
FOV
Field of view
FSE
Fast spin echo
FWE
Family-wise error
HAMA
Hamilton Anxiety Scale
HAMD
Hamilton Depression Scale
HC
Healthy controls
HMM
Hidden Markov model
HMM-MAR
Hidden Markov Model-Multivariate Autoregressive
LC
Locus coeruleus
LC_CNR
Contrast-to-noise ratio of the locus coeruleus
LIM
Limbic network
MCI
Mild cognitive impairment
MoCA
Montreal Cognitive Assessment
MSN
Morphological similarity network
NE
Norepinephrine
NEX
Number of excitations
NGF
Nerve growth factor

NM-MR
Neuromelanin-sensitive magnetic resonance
NM-MRI
Neuromelanin-sensitive magnetic resonance imaging
NMSS
Non-Motor Symptoms Scale
NPI
Neuropsychiatric Inventory
PD
Parkinson’s disease
PD-MCI
Parkinson’s disease with mild cognitive impairment
RBD
Rapid eye movement sleep behavior disorder
ROI
Region of interest
SBM
Surface-based morphometry
SCN
Structural covariance network
SMN
Somatomotor network
SNpc
Substantia nigra pars compacta
SNpc_CNR
Contrast-to-noise ratio of the substantia nigra pars compacta
TE
Echo time
TPN
Temporoparietal network
TR
Repetition time
UPDRS-III
Unified Parkinson’s Disease Rating Scale Part III
VAN
Ventral attention network
VBM
Voxel-based morphometry
Vis
Visual network

VisCent
Visual central network
VisPeri
Visual peripheral network.

Declarations

Competing Interests

The authors declare that they have no competing interests, or other interests that might be perceived to influence the results and/or discussion reported in this paper.

Ethics approval and consent to participate

The research protocol met ethical standards for research involving human participants and the study procedure was performed in accordance with relevant guidelines and regulations. The study was reviewed and approved by the Ethics Committee of Qilu Hospital, Shandong University (Approval number: KYLL-2021(ZM)-257). All participants gave their written informed consent before taking part in the study.

Consent for publication

Not applicable.

Funding

This research was supported by the National Key Research and Development Program of China (2022YFC2405100)and National Natural Science Foundation of China (82471265).

Author Contribution

Q. Liu wrote the main manuscript text and prepared all figures and tables. Z.Z. Zheng, W.C. Duan and Y.L. Xiao analysed and interpreted the data. L.H. Cui, P. Wang, F. Xue and Q.C. Cheng were major roles in the acquisition of data. T. Chen, F.G. Meng and R.H. Hou designed and conceptualized the study. All authors reviewed the manuscript.

Acknowledgement

We thank all the subjects involved in this study for their cooperation and contribution, as well as all our colleagues for their hard work and careful communication.

Data Availability

The data that support the findings of this study are available from the corresponding author upon reasonable request, due to ethical and privacy restrictions.

References

1. German DC, Manaye KF, White CL 3, et al. Disease-specific patterns of locus coeruleus cell loss[J]. Ann Neurol. 1992;32(5):667–76.
2. Braak H, Del Tredici K, Rüb U, et al. Staging of brain pathology related to sporadic Parkinson's disease[J]. Neurobiol Aging. 2003;24(2):197–211.
3. Weinshenker D. Long Road to Ruin: Noradrenergic Dysfunction in Neurodegenerative Disease[J]. Trends Neurosci. 2018;41(4):211–23.
4. Benarroch EE. The locus ceruleus norepinephrine system: functional organization and potential clinical significance[J]. Neurology. 2009;73(20):1699–704.
5. O'callaghan C, Hezemans FH, Ye R, et al. Locus coeruleus integrity and the effect of atomoxetine on response inhibition in Parkinson's disease[J]. Brain. 2021;144(8):2513–26.
6. Ehrminger M, Latimier A, Pyatigorskaya N, et al. The coeruleus/subcoeruleus complex in idiopathic rapid eye movement sleep behaviour disorder[J]. Brain. 2016;139(Pt 4):1180–8.
7. Moriya S, Yamashita A, Masukawa D, et al. Involvement of supralemniscal nucleus (B9) 5-HT neuronal system in nociceptive processing: a fiber photometry study[J]. Mol Brain. 2020;13(1):14.
8. Campos AC, P, Berzuino MB, Hernandes MS, et al. Monoaminergic regulation of nociceptive circuitry in a Parkinson's disease rat model[J]. Exp Neurol. 2019;318:12–21.
9. Kreiner G, Rafa-Zabłocka K, Barut J, et al. Stimulation of noradrenergic transmission by reboxetine is beneficial for a mouse model of progressive parkinsonism[J]. Sci Rep. 2019;9(1):5262.
10. Svenningsson P, Westman E, Ballard C, et al. Cognitive impairment in patients with Parkinson's disease: diagnosis, biomarkers, and treatment[J]. Lancet Neurol. 2012;11(8):697–707.
11. Hely MA, Reid WG, Adena MA, et al. The Sydney multicenter study of Parkinson's disease: the inevitability of dementia at 20 years[J]. Mov Disord. 2008;23(6):837–44.
12. Weintraub D, Simuni T, Caspell-Garcia C, et al. Cognitive performance and neuropsychiatric symptoms in early, untreated Parkinson's disease[J]. Mov Disord. 2015;30(7):919–27.
13. Aarsland D, Batzu L, Halliday GM, et al. Parkinson disease-associated cognitive impairment[J]. Nat Rev Dis Primers. 2021;7(1):47.
14. Rommelfanger KS, Weinshenker D, Norepinephrine. The redheaded stepchild of Parkinson's disease[J]. Biochem Pharmacol. 2007;74(2):177–90.
15. Healy CF, Brannigan AE, Connolly EM, et al. The effects of low-frequency endo-anal electrical stimulation on faecal incontinence: a prospective study[J]. Int J Colorectal Dis. 2006;21(8):802–6.

16. Speciale SG, Liang CL, Sonsalla PK, et al. The neurotoxin 1-methyl-4-phenylpyridinium is sequestered within neurons that contain the vesicular monoamine transporter[J]. Neuroscience. 1998;84(4):1177–85.
17. Srinivasan J, Schmidt WJ. Functional recovery of locus coeruleus noradrenergic neurons after DSP-4 lesion: effects on dopamine levels and neuroleptic induced-parkinsonian symptoms in rats[J]. J Neural Transm (Vienna). 2004;111(1):13–26.
18. Otto D, Unsicker K. FGF-2 modulates dopamine and dopamine-related striatal transmitter systems in the intact and MPTP-lesioned mouse[J]. Eur J Neurosci. 1993;5(7):927–32.
19. Sulzer D, Cassidy C, Horga G, et al. Neuromelanin detection by magnetic resonance imaging (MRI) and its promise as a biomarker for Parkinson's disease[J]. NPJ Parkinsons Dis. 2018;4:11.
20. Trujillo P, Aumann MA, Claassen DO. Neuromelanin-sensitive MRI as a promising biomarker of catecholamine function[J]. Brain. 2024;147(2):337–51.
21. Liu Q, Wang P, Liu C et al. An investigation of neuromelanin distribution in substantia nigra and locus coeruleus in patients with Parkinson’s disease using neuromelanin-sensitive MRI[J]. BMC Neurol, 2023, 23(1).
22. Maiti B, Koller JM, Snyder AZ, et al. Cognitive correlates of cerebellar resting-state functional connectivity in Parkinson disease[J]. Neurology. 2020;94(4):e384–96.
23. Hepp DH, Foncke EMJ, Olde Dubbelink KT, E, et al. Loss of Functional Connectivity in Patients with Parkinson Disease and Visual Hallucinations[J]. Radiology. 2017;285(3):896–903.
24. Zhang M, Zhou S, Wang H, et al. Unraveling morphological brain network disparities Parkinsonian tremor from essential tremor: an artificial intelligence approach for clinical differentiation[J]. NPJ Parkinsons Dis. 2025;11(1):253.
25. Zhang M, Zhou S, Yang P et al. The Precuneus Region Drives Brain Network Changes in Tremor-Dominant Parkinson's Disease: Insights from a Morphological Causal Analysis[J]. MedComm (2020), 2025, 6(11): e70441.
26. Sebenius I, Dorfschmidt L, Seidlitz J, et al. Structural MRI of brain similarity networks[J]. Nat Rev Neurosci. 2025;26(1):42–59.
27. Schaefer A, Kong R, Gordon EM, et al. Local-Global Parcellation of the Human Cerebral Cortex from Intrinsic Functional Connectivity MRI[J]. Cereb Cortex. 2018;28(9):3095–114.
28. Rubinov M, Sporns O. Complex network measures of brain connectivity: uses and interpretations[J]. NeuroImage. 2010;52(3):1059–69.
29. Vidaurre D, Abeysuriya R, Becker R, et al. Discovering dynamic brain networks from big data in rest and task[J]. NeuroImage. 2018;180(Pt B):646–56.
30. Wheelock MD, Strain JF, Mansfield P, et al. Brain network decoupling with increased serum neurofilament and reduced cognitive function in Alzheimer’s disease[J]. Brain. 2023;146(7):2928–43.

31. Železníková Ž, Nováková L, Vojtíšek L, et al. Early Changes in the Locus Coeruleus in Mild Cognitive Impairment with Lewy Bodies[J]. Mov Disord. 2025;40(2):276–84.
32. Falgàs N, Peña-González M, Val-Guardiola A, et al. Locus coeruleus integrity and neuropsychiatric symptoms in a cohort of early- and late-onset Alzheimer's disease[J]. Alzheimers Dement. 2024;20(9):6351–64.
33. Liu RP, Lin GL, Ma LL, et al. Changes of brain structure and structural covariance networks in Parkinson's disease associated cognitive impairment[J]. Front Aging Neurosci. 2024;16:1449276.
34. Wilson H, Niccolini F, Pellicano C, et al. Cortical thinning across Parkinson's disease stages and clinical correlates[J]. J Neurol Sci. 2019;398:31–8.
35. Sampedro F, Marín-Lahoz J, Martínez-Horta S, et al. Dopaminergic degeneration induces early posterior cortical thinning in Parkinson's disease[J]. Neurobiol Dis. 2019;124:29–35.
36. Haussmann R, Werner A, Gruschwitz A, et al. Precuneus Structure Changes in Amnestic Mild Cognitive Impairment[J]. Am J Alzheimers Dis Other Demen. 2017;32(1):22–6.
37. Yeo BT, Krienen FM, Sepulcre J, et al. The organization of the human cerebral cortex estimated by intrinsic functional connectivity[J]. J Neurophysiol. 2011;106(3):1125–65.
38. Herrington TM, Briscoe J, Eskandar E. Structural and Functional Network Dysfunction in Parkinson Disease[J]. Radiology. 2017;285(3):725–7.
39. Berman BD, Smucny J, Wylie KP, et al. Levodopa modulates small-world architecture of functional brain networks in Parkinson's disease[J]. Mov Disord. 2016;31(11):1676–84.
40. Alexander-Bloch A, Giedd JN, Bullmore E. Imaging structural co-variance between human brain regions[J]. Nat Rev Neurosci. 2013;14(5):322–36.
41. Vidaurre D, Smith SM, Woolrich MW. Brain network dynamics are hierarchically organized in time[J]. Proc Natl Acad Sci U S A. 2017;114(48):12827–32.
42. Vidaurre D, Hunt LT, Quinn AJ, et al. Spontaneous cortical activity transiently organises into frequency specific phase-coupling networks[J]. Nat Commun. 2018;9(1):2987.
43. Nasreddine ZS, Phillips NA, Bédirian V, et al. The Montreal Cognitive Assessment, MoCA: a brief screening tool for mild cognitive impairment[J]. J Am Geriatr Soc. 2005;53(4):695–9.
44. Hamilton M. A rating scale for depression[J]. J Neurol Neurosurg Psychiatry. 1960;23(1):56–62.
45. Hamilton M. The assessment of anxiety states by rating[J]. Br J Med Psychol. 1959;32(1):50–5.
46. Morris JC. The Clinical Dementia Rating (CDR): current version and scoring rules[J]. Neurology. 1993;43(11):2412–4.
47. Cummings JL, Mega M, Gray K, et al. The Neuropsychiatric Inventory: comprehensive assessment of psychopathology in dementia[J]. Neurology. 1994;44(12):2308–14.
48. Rosen WG, Mohs RC, Davis KL. A new rating scale for Alzheimer's disease[J]. Am J Psychiatry. 1984;141(11):1356–64.
49. Katz S, Ford AB, Moskowitz RW, et al. STUDIES OF ILLNESS IN THE AGED. THE INDEX OF ADL: A STANDARDIZED MEASURE OF BIOLOGICAL AND PSYCHOSOCIAL FUNCTION[J]. JAMA.

1963;185:914–9.

50. Goetz CG, Tilley BC, Shaftman SR, et al. Movement Disorder Society-sponsored revision of the Unified Parkinson's Disease Rating Scale (MDS-UPDRS): scale presentation and clinimetric testing results[J]. Mov Disord. 2008;23(15):2129–70.
51. Chaudhuri KR, Martinez-Martin P, Brown RG, et al. The metric properties of a novel non-motor symptoms scale for Parkinson's disease: Results from an international pilot study[J]. Mov Disord. 2007;22(13):1901–11.

Figures

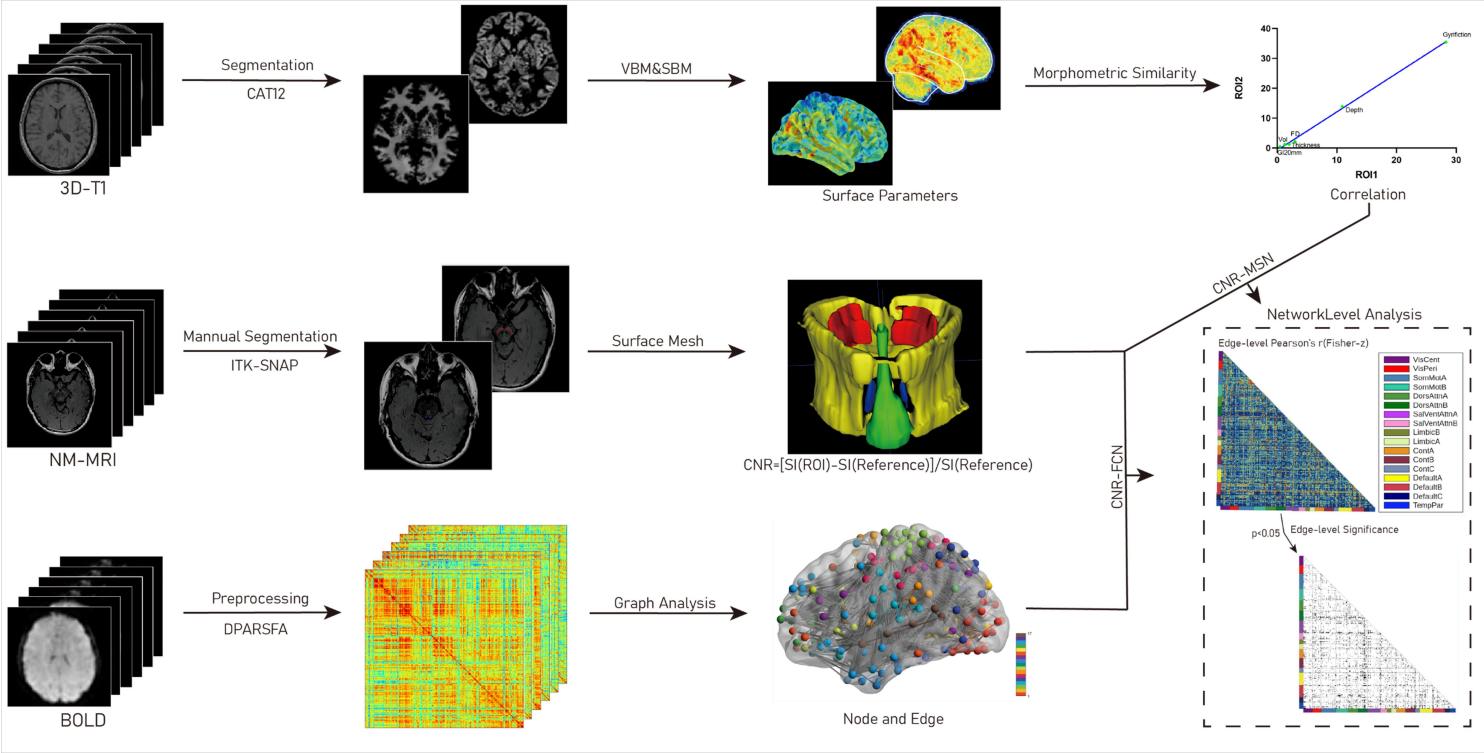


Figure 1

MRI Data Preprocessing and Analysis Pipeline. CNR: contrast-to-noise ratio. SI(ROI): signal intensity of target area. SI(Reference): signal intensity of reference area. FC: functional connectivity. CNR-FC(r) Network: the correlation coefficient matrix between CNR and FC. VisCent: Visual Central Network; VisPeri: Visual Peripheral Network; SomMotA/SomMotB: Somatomotor Network A/B; DorsAttnA/DorsAttnB: Dorsal Attention Network A/B; SalVentAttnA/SalVentAttnB: Salience/Ventral Attention Network A/B; LimbicA/LimbicB: Limbic Network A/B; ContA/ContB/ContC: Control Network A/B/C；DefaultA/DefaultB/DefaultC: Default Mode Network A/B/C; TempPar: Temporal Parietal Network.

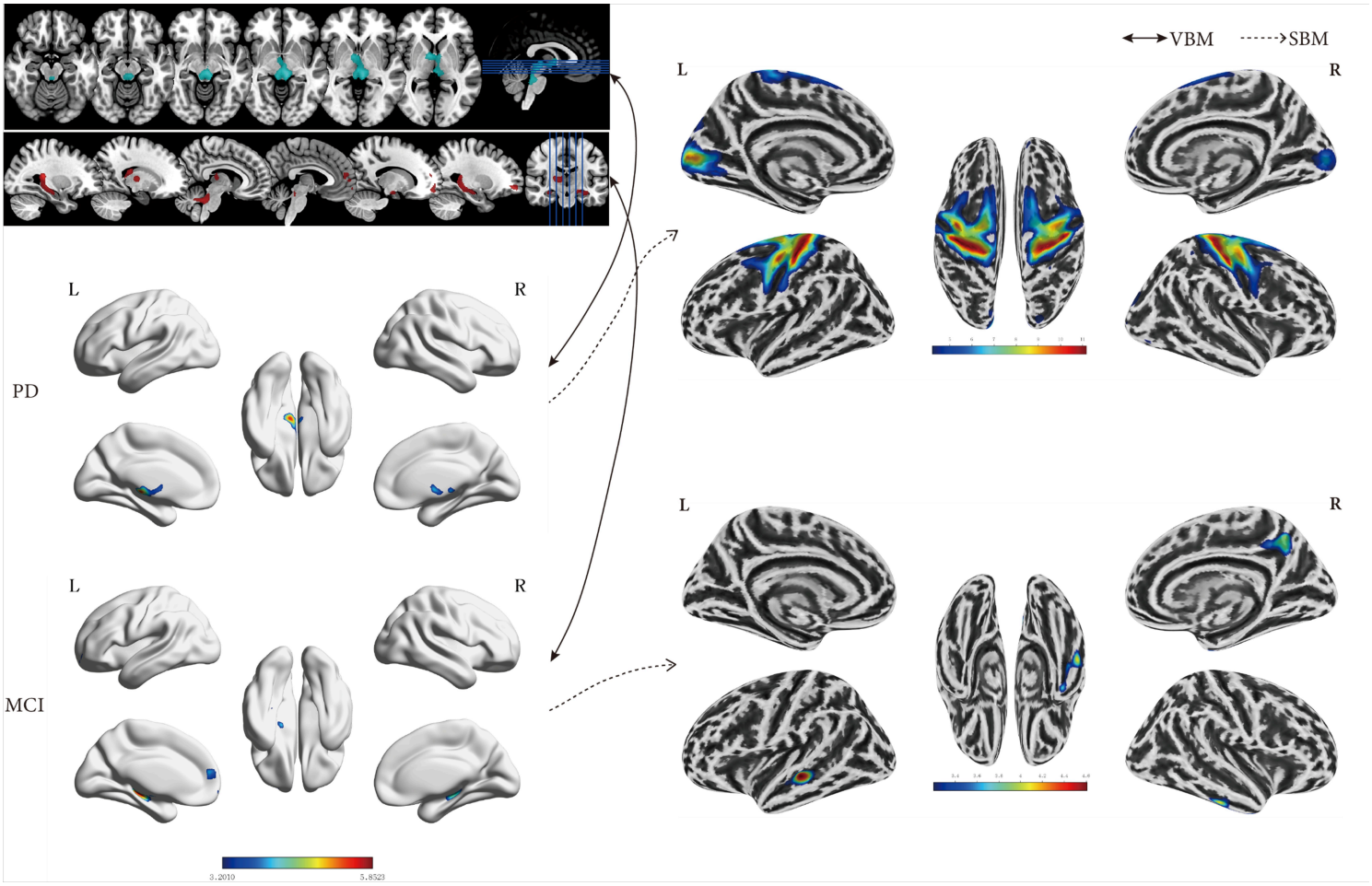


Figure 2

The results of VBM and SBM analysis. VBM: Voxel-based morphometry analysis. SBM: Surface-based morphometry analysis. The colorbars represent T values.

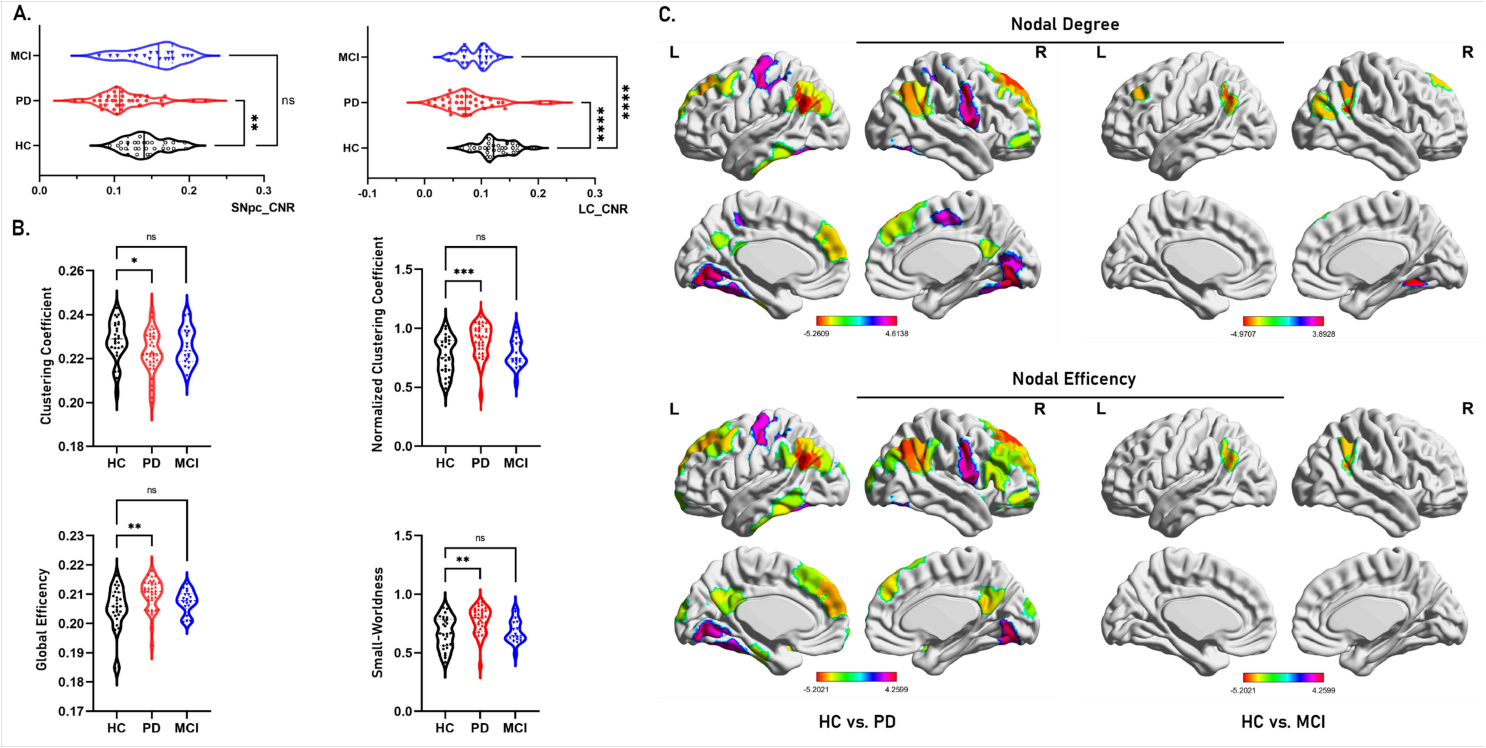


Figure 3

A.: The results of CNR on NM-MRI; B.: The analysis of global network metrics; C.: The analysis of nodal network metrics. The colorbars represent T values.

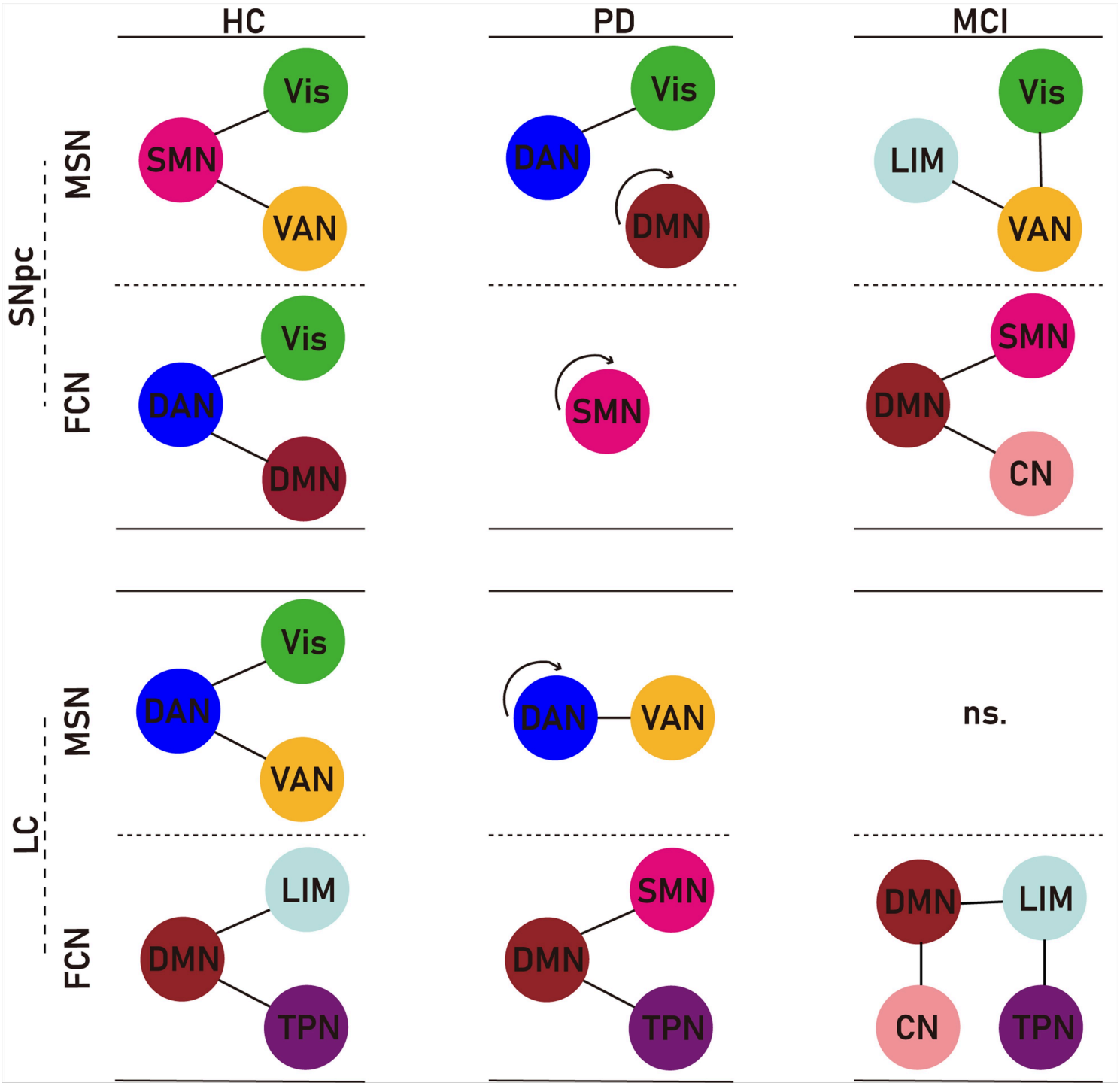


Figure 4

Network-level analysis of substantia nigra pars compacta (SNpc) and locus coeruleus (LC) on morphological similarity network (MSN) and functional connectivity network (FCN). Vis: Visual network; SMN: Somatomotor network; DAN: Dorsal attention network; VAN: Ventral attention network; LIM: Limbic network; CN: Control network; DMN: Default mode network; TPN: Temporoparietal network. ns. means none of significance. The circles represent network modules, the connecting lines indicate inter-network coupling, and the arcs denote intra-network coupling.

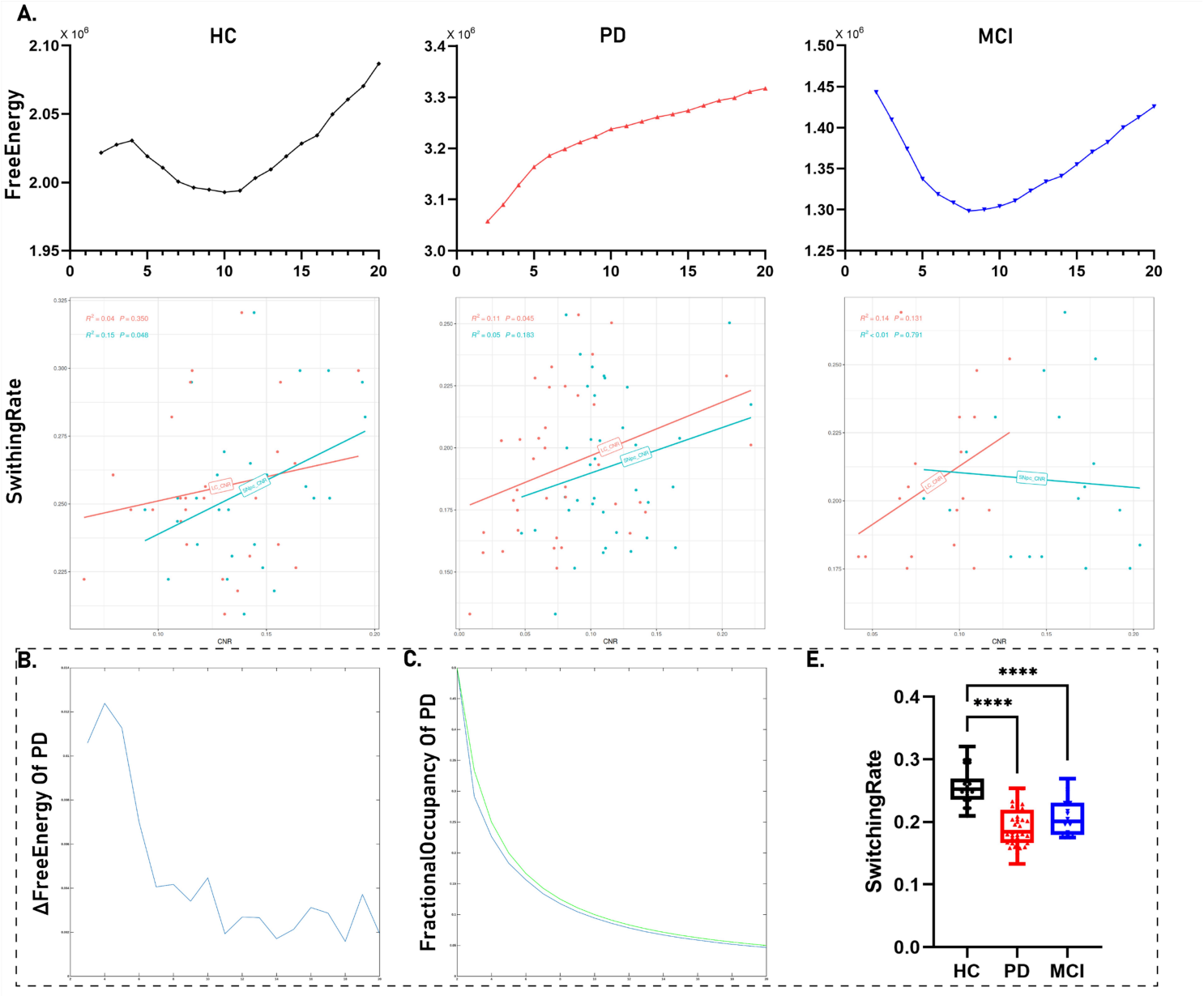


Figure 5

A.: The variation in mean free energy (FE) as a function of the state number in the Hidden Markov model (HMM), and the regression analyses of state transition rates with SNpc_CNR and LC_CNR; B.: The relative free energy gain between adjacent state numbers (ΔFE/FE) in PD group; C. The blue line means the variation in mean fractional occupancy (FO) as a function of the state number in PD's HMM and the green line means the reciprocal of the state number (1/K); E. The analysis of switching rates between groups.

Supplementary Files

This is a list of supplementary files associated with this preprint. Click to download.

- Table1.docx

- Appendix1a.png
- Appendix1b.png
- Appendix2c.png
- Appendix2b.png
- Appendix2a.png